Image Quality Analysis in Dual-Source CT

by

David Solano Solano

Submitted to the Mannheim Medical Faculty
in partial fulfillment of the requirements for the degree of

Master of Science

at the

UNIVERSITY OF HEIDELBERG

August 2008

Signature of Author .....
Mannheim Medical Faculty
January 28, 2009

Certified by .....
PD Dr. med. Dipl. Phys. Gerald Weisser
Clinical Radiology and Nuclear Medicine Section, Quality Management and Imaging Informatics
Associated Professor of Radiology

Accepted by .....
Prof. Dr. med Fredrerik Wenz
Director, Clinic of Radiotherapy and Radiooncology

Contents

List of Figures

List of Tables

Abstract

Dual Source CT (DSCT) is new CT medical application, in which three sets of image data can be obtained by two independent X ray tubes to achieve a better tissue differentiation. In the present work, the noise, low contrast and high resolution behavior is measured for the Siemens® DSCT system Definition^{TM} and then compared with other model of the Somaton^{TM} series. The modern 64-slices detector technology implemented within the Definition^{TM} produces a relatively large scattered radiation that affects significantly the distinction of low density difference regions and increases the presence of noise. An non uniform illumination anomaly is found in the images obtained in the dual mode of the scanner. Although the z-axis resolution has strongly improve, the noisy character of the DSCT brings a step back in terms of xy-resolution. The use of this of type of scanner is therefore recommended for high speed and thin slice studies.

Chapter 1

Introduction

Dual source computed tomography (or *DSCT*) was introduced in 2005 [1] and offers to the radiologist the possibility of obtaining images with an improved tissue differentiation due the simultaneous data acquisition from two different X ray sources. By the present time, several clinical applications has tested the advantages of this newly introduced system, like cardiac CT ([2]) and coronary angiography CT ([3]). Because this new kind of CT system implements dozen multislices technology ([4], [5] and [6]), its main advantanges are fast scannings, thin slice and enhanced image quality for small details.

Although DSCT systems are frequently reviewed as an improvement in soft tissue differentiation and resolution, some radiognostics physicians have addressed the issue of the image quality when compared to previous models with one single tube and less slices per rotation. Then, the recent advances in scanning speed seem to hide some problems than other older scanner with simpler detector arrays probed to handle in more efficient ways.

The presentation of this research aims to answer those questions of the image quality in concrete fashion by means of concise numerical results. The goals pursued in [4] are amplied here in a more mathematical and physically precise way that could be more accesible to designers, engineers and physicists, therefore the approach is less clinically oriented.

The present work shows the results of a series of trials that tested the performance limits in terms of image quality of a commercial DSCT system. To achieve this objetice, a twofold strategy is chosen. At first, a specially designed phantom with materials with low electron density is employed to test the low contrast behavior of regular clinical setups. Image-related

and statistical variables –like contrast and noise– are looked to be associated with physical phenomena, so it could be possible to stablish a measurable conection with physical observables. Later, the highest tridimensional resolution of the scanner is meassured by mean of a phantom with a millimeter-sized metal bead embedded in a material density. By doing so, it is possible to get the dimension of the smallest object that the scanner can detect and process in regularly employed clinical configuration. Those tests are performed also in other multi-slice CT systems of the same manufacturer in order to compare the results.

Chapter 2

Materials and Methods of Analysis

2.1 Scanners

In the present work, three scanners from the SOMATON™ series manufactured by Siemens®[1] were used. The models included the newly released double-source computer tomography system Definition™ and the single source scanners Emotion 16™ and Volume Zoom™.

Features	**Volume Zoom™**	**Emotion 16™**	**Definition™**
Slices per rotation	4	16	64
Rotation time (ms)	500	600	330
Spatial Resolution (lp/cm)	30	30	42
Recontruction Time (slides/s)	1.5	16	20

Table 2.1: Scanners from the Siemens® SOMATON™ series and its technical specifications.

As the Emotion 16™ and Volume Zoom™ are standard multi-slice computed tomography systems, here is discussed only and briefly the Definition™ scanner because of its innovative double X ray tube design (for example [1]) . The *DSCT* is composed of two X ray sources with an angular offset of 90^o and their respective detectors. One detector covers an entire scan field of view of 50 *cm* in diameter, while the other detector is restricted to a smaller, central, 26 *cm* in diameter, field of view due to space limitations of the gantry. Each detector comprises 40

[1]Siemens AG, Healthcare Sector. Address: Henkestrasse 127, D-91052 Erlangen, Germany. In the internet: http://www.medical.siemens.com/

detector rows, where the central 32 ones have a 0.6 mm collimated slice width and the outer rows (on both sides) a 1.2 mm collimated slice width. The total coverage in the z-axis of each detector is 28.8 mm in the isocenter. Using the z-flying focal spot technique ([6] and [5]), two subsequent 32−slice readings with 0.6 mm collimated slice width are combined to one 64−slice projection with a sampling distance of 0.3 mm at the isocenter. By this way, each detector acquires 64 overlapping 0.6 mm slice per rotation. As it can be seen in the Table 2.1, the minimal gantry rotation is of 0.33 s, although the system can also be perform larger rotations times of 0.5 s and 0.1 s. Both the Siemens® STRATON^{TM} X ray tubes [7] allows up to 80kW peak power from the two on-board generators, so each tube can be operated independently with regard to their kilovolt and milliampere configurations.

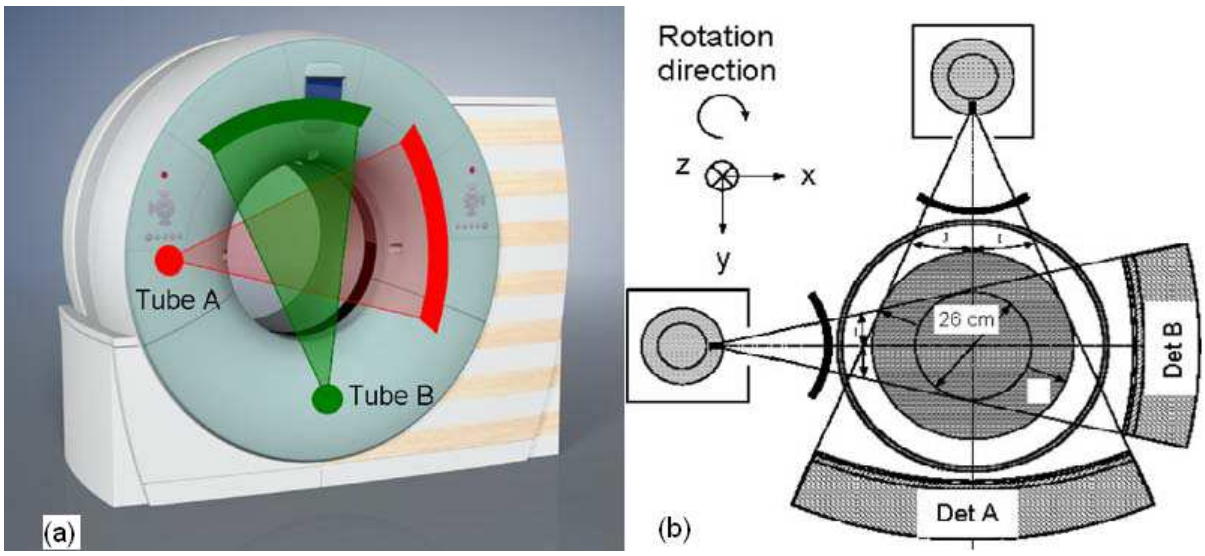

Figure 2-1: Due to space limitations in the gantry, the detector set for the tube "A" allows a full field of view of 50 cm diameter, while for the tube-dectector system "B" only a 26 cm one.

The Definition^{TM} DSCT system can be used both as single-source and dual-source mode. When it is set to single source-mode, its image stacks do not have significant differences in term of data storage in hardware devices and file structure with its conventional CT counterparts like Emotion 16^{TM} and Volume Zoom^{TM} (the DICOM framework is used as a standard, too). But when it is configured properly in dual energy mode, the computer system generate three image sets: one for each tube (which was set at certain kilovolt) and additional dual stack that

comprises features from both sources.

2.2 Phantom

The Catphan412x412 (manufactured by The Phantom Laboratories®[2]) with the special modules CTP528 for high resolution studies and the CPT515 for low resolution test.

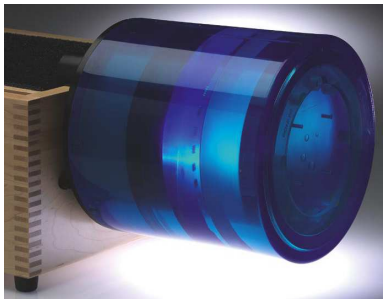

Figure 2-2: Catphan412x412™ is a tool for advaced quality assurance tests in modern CT scanners. (Image cortesy from The Phantom Laboratory, New York, USA).

As shown in Figure 2-3 , the CTP515 Low Contrast module [8] includes the so-called supra-slice targets (with $z-$dimension longer than most maximum slice width) and sub-slice targets (with $z-$axis length smaller than more of the usual slice width). In other words, the sub-slice targets are only visible on very few images of the stack. Because of the larger number of supra-slice target among the image set, they represent a better source of statistical samples for the present study and they are used exclusively among all this report. The low contrast targets diameters of the supra-slice set are: $2.0\,mm$, $3.0\,mm$, $4.00\,mm$, $5.00\,mm$, $6.00\,mm$, $7.00\,mm$, $8.00\,mm$, $9.0\,mm$ and $15.0\,mm$; and for sub-slice ones: $3.0\,mm$, $5.00\,mm$, $7.00\,mm$ and $9.00mm$. There are 3 nominal contrast percent for both the supra and sub- slice targets: 1%, 0.5% and 0.3%, and their actual values need to be determined before running specific contrast performance tests. A target with nominal value "$a\%$" is a ROI where there difference between its average gray value and that of the background (within a ROI with equal dimensions) is roughly $a\%$. Since there is a proportionality relation between gray values (or Houndsfield units) to electron

[2]The Phantom Laboratory P.O. Box 511, Salem, NY 12865-0511 USA. In the internet: http://www.phantomlab.com/

density, the nominal value of the target or *field* (as it will be frequently called in the present work) also describes a quantitative measure of its constituent material density with relation to the one of the sustrate in which it is embedded.

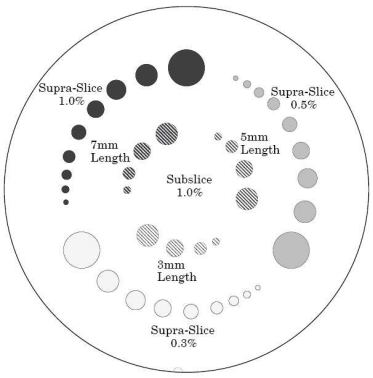

Figure 2-3: The CTP515 low contrast odule of the CATPHAM from The Phantom Laboratories. The inner (smaller) circle of field are sub-slice targets and the those located in the outer (larger) outline are the supra-slice targets.

The CTP528 High Resolution module has a 1 through 21 line pair per centimeter high resolution test gauge and an impulse source (bead) which is cast into a uniform material (Figure 2-4). The bead is made from tungsten carbide, its diameter is of 0.28 mm and is positioned along 21 mm above the phantom's center and 10 mm past the center of the auge in the z direction.The 1 through 21 line pair gauge is not used in this study, so the CTP445 module could be used perfectly instead.

2.3 Image Analysis

2.3.1 Low Contrast Tests

For the low contrast tests, a *Region of Interest* or *ROI* is a particular circular selection inside a image which diameter is 10 mm. Each image of the scanned CTP515 module must contain four ROI's: 3 for "$a\%$" contrast fields and 1 for the background field, where $a = 1, 0.5$ and 0.3. The *contrast fields* of interest in this study will be defined as the 15 mm-diameter supra-slice targets, where a slight difference of density is represented as a larger and observable mean gray

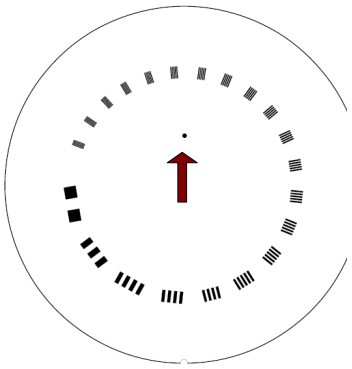

Figure 2-4: The CTP528 high resolution module with an impulse signal bead (pointed by the red arroy) and 1 to 21 line per centimeter gauge set. The size of the bead has been widely enlarged for illustration purposes.

value. The smaller circular regions (smaller supra-slice or sub-slice targets) with similar density contain equivalent data, but not as statistically significant as the largest ones because of the larger frequency of noise within them. So the choice of the 15 mm diameter contrast fields as the ROI's in the data analysis is based on their smaller noise influence. The ROIS's must contain the largest number of pixel samples, that is, the limiting circle of the selection must be the outer contour of the contrast field, as shown in Figure 2-5.

The *background field* is defined as 10 mm diameter circular region in an arbitrary position (Figure 2-5) that does not overlap with any of the sub or supra- slice targets and represents a measure of the background generated signal.

Now, let be the $G_{a\ i}$ the mean gray value of the a % contrast field and $G_{b\ i}$ the mean gray value of the background in the i-th image of the stack. If the stack is made of M images, then mean value of a % contrast field and the background field are, respectively:

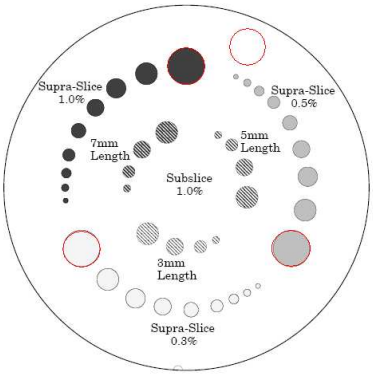

Figure 2-5: Regions of Interest (ROI's) in a CTP515 module sample slice. Optimal ROI'S selection must contain the largest number of pixel inside the largest higher density circles. An aditional ROI (in the top right) is made to perform statitics calculation of the background noise.

$$G_a = \frac{1}{M}\sum_{i=1}^{M} G_{a\ i} \tag{2.1}$$

$$G_b = \frac{1}{M}\sum_{i=1}^{M} G_{b\ i}. \tag{2.2}$$

The *contrast definition* at the $a\%$ field, which measures the actual signal generated by the X-rays on the detector, is defined as the difference

$$C_a \equiv G_a - G_b. \tag{2.3}$$

The standard deviation is the measure of the noise in this work. So, let $\sigma_{a\ i}$ and $\sigma_{b\ i}$ the standard deviation for the $a\%$ contrast and the background fields, respectively. Therefore, the associated noise for the stack of M image is defined as the mean value of the standard deviations:

$$\sigma_a = \frac{1}{M}\sum_{i=1}^{M}\sigma_{a\ i} \tag{2.4}$$

$$\sigma_b = \frac{1}{M}\sum_{i=1}^{M}\sigma_{b\ i}. \tag{2.5}$$

The *noise definition* (or just *noise*) of the stack is defined as the "euclidean" magnitude of both the standard deviations of the contrast field and the background:

$$N_a \equiv \sqrt{\sigma_a^2 + \sigma_b^2} \tag{2.6}$$

Finally, the *signal-to-noise ratio* at the a % contrast field, R_a, a measure of how important is the noise in the image, is defined as

$$R_a \equiv \frac{C_a}{N_a}. \tag{2.7}$$

2.3.2 High Contrast Tests

For the high resolution performance evaluations, here is followed the standard procedure in [10], that consists in the plotting of the z and xy- axis profile and then the computation of the corresponding Full Width at the Half Maximum for both signals.

The z-axis profile is constructed by finding the greatest gray intensity inside a small fixed ROI (of 3 mm) that contains the impulse signal of the CTP528 module. It is important to compute the maximum from the fixed ROI in slices that are "after" and "before" the impulse appearance. For image sets obtained from the same session[3], the z-axis profile must have the same starting and finishing slice, so each sample stack can be comparable with others. Let z_i the location of the i-th slice and $G_{\max\ i}$ its corresponding maximum intensity inside the ROI, so the *measured z-axis* profile Z is the set of M pairs:

[3]Here *session* is a series of studies with same scanner and the same table setup for a short lapse of time.

$$Z = \{(z_i, G_{\max\ i}) \backslash i = 1..M\} \tag{2.8}$$

Without lost of generalty, the value of z_1 can be set as 0, and if the slice separation is Δz, then the location of the i-th slice is easily found as: $z_i = i \cdot \Delta z$. For all the high contrast test, the slice separtion had been set to its nominal minimum, so the evaluation of the scanner be in the limit of its factory performance. The set of pairs Z is fitted to a Gaussian function of the form:

$$g_1(z) = a_1 e^{-(z-a_2)^2/a_3^2} + a_4 \tag{2.9}$$

by means of a conventional least squares method. There is subtle difference between slice thickness and slice separation. In general, the lowest nonimal slice thickness are around 1 mm, but the slice separation is far less, therefore is a overlapping. In order to perform an appropiate optimization program, a reasonable set of ranges must be set for each of the parameter a_1, a_2, a_3 and a_4. For the a_1 parameter (the amplitude of the wave impulse), the minimum was set as $0.5G_{\max}$ where:

$$G_{\max} = Max\{G_{\max\ i} \backslash i = 1..M\}, \tag{2.10}$$

so the minimum of the amplitude in the optimization problem is set as the 50% of the greatest intensity of the measured z-profile. In a similar fashion, the maximum was set as $1.5G_{\max}$, and therefore $A_1 \in]0.5G_{\max}, 1.5G_{\max}[$. Let $L = M \cdot \Delta z$ the total length of the sample in the z direction. The a_2 parameter is the location of the intensity peak, it is easy to see that $a_2 \in]0, L[$. For the a_3 parameter, which is related to the "standard deviation" of the signal and ergo to the full width at the half maximum, must be somewhere between total length of the set L (as the upper limit) and some minimal thickness $\alpha \cdot \Delta z$ (as the lower limit), where α is arbitrary positive scalar freely to choose but no greater than 1. The "educated guess" $\alpha = 0.3$

was chosen for simplicity, so $a_3 \in]0.3{\cdot}\Delta z, L[$. Finally, a_4 represent the offset of the Gaussian curve from the z-axis. As the gray intensity of 0 is minimum possible (and reasonable) for a typical CT image, the range for the offset a_4 was set as $]0, 0.1G_{\max}[$. The correct definition of the offset a_4 is very important to compute a good fitting of the profile, if the bottom guess would be set as $G_{\min} = Min\{G_{\max\ i} \backslash i = 1..M\}$, it is possible to get a negative gray intensity value due to some "anomalous" pixels that exist in some image and then the optimization problem would be ill-posed.

Once the fitting is gotten from the optimization problem, simple algebra shows that the Full Width at Half Maximum on the z-direction based on the Gaussian model is:

$$FWHM_z = 2B_1 \ln 2, \tag{2.11}$$

which is a measure of the highest possible resolution of the scanner in the longitudinal degree of freedom, or in another words, the real minimal slice thickness.

For xy-plane profile, let k the slide number of that has the peak maximum intensity so that $G_{\max\ k} = G_{\max}$. In that particular k slice a squared-shaped ROI is made so that the complete area of the impulse signal is contained within. The square shape of this ROI is due to its simplicity and its direct representation in rectangular coordinates, although equivalent results can be obtained with circled-shape ROI's. This selected region will be a rectangular grid where each pair (x_i, y_i) is associated to a gray intensity G_i^{grid}. Therefore, in a similar fashion to the eq. 2.8 and 2.9, a set of triads:

$$W = \{\left(x_i, y_i, G_i^{grid}\right) \backslash i = 1..M^{grid}\} \tag{2.12}$$

(where M^{grid} is the number of pixels in the ROI) is meant to be fitted to a 2-dimensional Gaussian pulse with elliptical cross section of the form:

$$g_2\left(x, y\right) = b_1 e^{-\left((x-b_2)^2/b_3^2 + (y-b_4)^2/b_5^2\right)} + b_6. \tag{2.13}$$

As well as in the z-profile fitting problem, the ranges of parameters $b_1, b_2, b_3, b_4, b_5, b_6$ must be properly chosen in order to get reasonable results. Now, let S the side length of the square-shaped ROI and $W_\partial = \{(\bar{x}, \bar{y}), (\bar{x}+S, \bar{y}), (\bar{x}, \bar{y}+S), (\bar{x}+S, \bar{y}+S)\}$ the four vertex of the selection and by following similar arguments than for the z-profile model, the ranges for the xy-model were set as:

$$\begin{aligned} b_1 &\in]0.5G_{\max}, 1.5G_{\max}[\,, \\ b_2 &\in]\bar{x}, \bar{x}+S[\,, \\ b_3 &\in]0.01S, S[\,, \\ b_4 &\in]\bar{y}, \bar{y}+S[\,, \\ b_5 &\in]0.01S, S[\\ b_6 &\in]0, 0.1G_{\max}[\,. \end{aligned} \tag{2.14}$$

Particular interest has the geometry of the ellipse produced by the intersection of $g_2(x, y)$ and the plane $g = b_1/2$. If $b_3 > b_5$ (so that larger axis of the ellipse is on the x direction), then the perimeter of the ellipse P is by elementary analysis

$$P = 4\pi b_3 E\left(\sqrt{1-\left(\frac{b_5}{b_3}\right)^2}\right), \tag{2.15}$$

where $E(x)$ is the complete elliptical function of the second type of the real variable "x". The ratio b_3/b_5 is a measure of the "circularity" of the signal, that means, the closer is the ratio is to 1, the better fitted as a circle the scanned bead is. Since in general all the pulse signal are very close to the circle geometry, an "average" measure pulse spread in any direction is given by P/π, so that the Full Width at the Half Maximum[4] at the xy-plane is defined all over the present work as:

[4]Naturally if $b_3 < b_5$, then the ratio must inverted and $FWHM_{xy} = 4b_5 E\sqrt{1-\left(\frac{b_3}{b_5}\right)^2}$.

$$FWHM_{xy} \equiv 4b_3 E\left(\sqrt{1-\left(\frac{b_5}{b_3}\right)^2}\right). \tag{2.16}$$

A important issue in DSCT imaging is the relative location of areas of interest between the three image sets generated by the system. This relative displacement can be defined mathematically in the following way. Let be $T_1 \subseteq S_1$ a region of clinical interest in the image set S_1 and $\vec{r}_1$ a point in it so that $\vec{r}_1 \in T_1$. Therefore, there is relative rotation and translation between the image set S_1 and S_2 if for the region $T_2 \subseteq S_2$ it holds that $T_2 = \{\vec{r}_2 \in S_2 / \vec{r}_2 = A\vec{r}_1 + \vec{a}\}$, where A is rotation matrix and $\vec{a}$ is a traslation vector. Rigorously, there must be an homomorphism between the subsets T_1 and T_2 and a series of complex criteria that can ensure that those regions correspond clinically to the same anatomical structure (like intensity values, shape, volume, etc), but for the present analysis those considerations are not very important, so it is not very necessary to swim those deep waters by now. In other words, given a clinically important point in the image set S_1 located at $\vec{r}_1$, there is displacement $\Delta\vec{r}$ relative to image set S_2, so that that same anatomical structure is positioned in the image set S_2 at $\vec{x}_2 = \Delta\vec{r} + \vec{r}_2$. The study of the relative displacement between image sets in dual mode is done here by the following bead center analysis.

By taking in consideration all the parameters of both the z-axis profile xy-plane profile models, the point where the highest intensity value is found in all the stack is given by:

$$\vec{r}_c = (x_c,\ y_c,\ z_c) = (a_2, b_2, b_4)\,, \tag{2.17}$$

where the model parameter a_2, b_2, b_4 are defined in eq. 2.9 and 2.13 respectively. Hence, these coordinates correspond to the position of the geometric center of the metal bead. The bead center between the different tube energy stacks is compared in the Results chapter.

2.4 Computation Tools

A pair of programs in the *ImageJ*[5] ([11], [12]) macro language (a version of Java specially designed for image manipulation) was written to process the statistical measures of the stacks (like in-ROI contrast and noise definition, signal-to-noise ratio, maximum gray intensities, etc.). The automatic extraction of the statistics is programmed in such a way that the positioning of the ROI be completely invariant for images sets that come from the same session. Further data analysis, like graphs and fitting optimization problems were done in Maple^{TM} 10[6].

[5] *ImageJ is developed at the National Institutes of Health (NIH) of the United States of America. Its official web site is found at: http://rsbweb.nih.gov/ij/*

[6] Maple^{TM} is a computer algebra interface manufactured by MapleSoft® (615 Kumpf Drive, Waterloo, Ontario, Canada N2V IK8). In the internet: http://www.maplesoft.com.

Chapter 3

Results

3.1 General Organization

For the purpose of image quality analysis in the present work, the CTP515 and CTP528 modules of the Catphan$^{\text{TM}}$ were used in each of the scanners of the Table 2.1.

For specific case of the low contrast performance tests, several kernels were used to reconstruct the data in both abdomen and head field of view (FOV), which are respectively $350cm \times 350cm$ and $250cm \times 250cm$. Because the head studies are usually oriented to soft tissue diagnostics, the doses (tube currents) are generally higher than the abdomen ones.

The dose related physical observable used along the present work is the *Volume CT Dose Index* or $CTDIvol$, which is defined as:

$$CTDIvol = (1/KTp)\left(\frac{1}{3}\int_{-50mm}^{50mm} D_c\,(z)\,dz + \frac{2}{3}\int_{-50mm}^{50mm} D_p\,(z)\,dz\right) \tag{3.1}$$

where $D_c(z)$ is the dose profile over the z-axis in water phantom in the center $D_p(z)$ the dose profile on periphery, K number of slices per collimation (for instance, $K = 4,\ 16,\ 32$ for the Volume Zoom$^{\text{TM}}$, Emotion 16$^{\text{TM}}$ and Definition$^{\text{TM}}$ with flying focal spot technic, respectively), T the slice thickness in mm and p the pitch[1] ([9] and [4]). In general, any single physical

[1]The pitch is Spiral CT related concept. It is defined as the ratio between the table speed v and the number of slices per collimation K and the slice nominal width T: $p \equiv v/KT$.

quantity directly related to the dose D is also to the $CTDIvol$.

For each FOV mode and reconstruction kernel, several image sets at different $CTDIvol$ were obtained. The number of image sets per FOV per kernel ranges from 3 to 10 samples, each one at one different tube current (which corresponds to a specific $CTDIvol$) at a constant cathode kilovolt, generally of 120 kV for the Definition™ and Volume Zoom™ and 130 kV for the Emotion 16™. Due to the particular dual source features of the Definition™, the pair of kilovolt values 80 kV/140 kV was always used along both low contrast and high contrast studies when the scanner was in dual energy mode. Table 3.1 shows an overview of this particular data hierarchy.

The high contrast trials were performed only in the head mode because this particular FOV allows a more clear characterization of small details due its smaller pixel size ($\sim 0.49\ mm$, while for the Abdomen mode $\sim 0.68\ mm$). In the Table 3.2 it is shown which reconstruction kernels were used in the high contrast tests.

FOV/Scanner	*Definition™*	*Emotion 16™*	*Volume Zoom™*
Abdomen	b30f, b31f	b30f	b30f
Head	b30f, b31f, h30s, h31s, h60s	h30s, h31s	b30f, h30s

Table 3.1: Reconstruction kernels used for the low contrast tests by the CT systems each scanner and FOV. The b30f and b31f kernels in the head FOV were used in the dual energy mode of the Definition™.

Kernel/Scanner	*Definition™*	*Emotion 16™*	*Volume Zoom™*
b31f	•		
b70f	•	•	
*h45*s			•

Table 3.2: Used kernels in the high contrast tests. The two image sets that come from the Definition™are in dual energy mode.

3.2 Low Contrast Tests

3.2.1 Contrast Definition

One of the special features of the Catpham^{TM} phantom is a highly uniform contrast independently from the input kilovolt or tube current [8]. This important characteristic of the phantom design was used to verify the perfomance of the DSCT system Definition^{TM} and then to compare it with the older single tube scanners.

In the Figure 3-1 it is shown the contrast measures (as described in p.8) in the stacks generated by the three used scanners with the $300mm \times 300mm$ Abdomen FOV. Each data set was reconstructed with the B30F. The kilovolt was set to 120 kV in the Definition^{TM} and Volume Zoom^{TM} scanners and to 130 kV in the Emotion 16^{TM} system. In this particular test, the Definition^{TM} scanner functioned as a standard single-sourced scanner. In general, each stack contained slices with a $3mm$ slice thickness.

In a similar fashion, analogous measures of contrast were made in similar data stacks in $250mm \times 250mm$ head FOV mode (Figure 3-2). The kilovolt configuration was set much alike the tests runned in abdomen FOV described in the last parragraph. In this particular series of studies, the reconstruction kernel used was the clinically frequently used H30S. Every slice in all samples has a $5mm$ slice thickness.

In Figure 3-3, it is shown the contrast in data sets obtained from the Definition^{TM} scanner in single mode. In this particular test, the performace of the DSCT system is evaluated with different head reconstruction kernels. The purpose of this part of the study is to check the consistentency of the reconstructed image sets according to the kernel nomenclature. Here is briefly reviewed the kernel naming system. For a kernel with name "*[Type]XS*" –where *[Type]* can be H for head or B for body studies and "X" a integral number–, high difference in gray values between regions of the image will be amplified as the value of *"X"* increases. This study can provide useful information to the physician about which kernel is appropiate to include in routine diagnostic procedures that make use of the DSCT with 64-slice detector design. The issue of DSCT-specific settings in the clinical study protocol will be revisited in the following chapters again.

The contrast check in the Definition^{TM} dual source mode is shown in Figure 3-4. B30F

and B31F were used as reconstruction kernels in Head FOV. Each graph shows the obtained measures from data sets generated from sources at 80 kV and 140 kV and the additional stacks generated by making use of both sources. These special, new-featured data sets will be named as "*Dual*" along the present work.

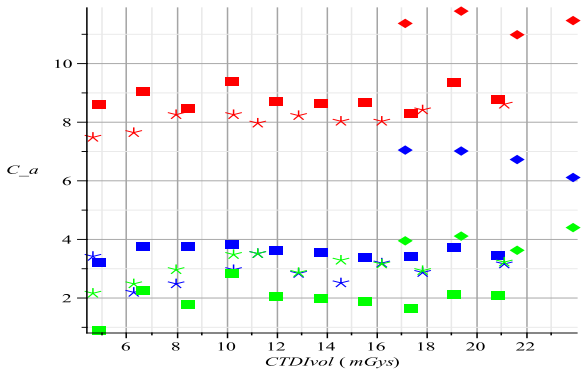

Figure 3-1: Contrast against CTDIvol (in mGys) from data sets processed by the Definition^{TM} (*asterisks*), Emotion 16^{TM} (*squares*) and Volume Zoom^{TM} (*diamonds*) systems in Abdomen FOV. The kernel B30F was used for the reconstruction. The color key is red for the 1 % contrast fields, blue for 0.5 % and green for the 0.3 %.

3.2.2 Instability in the Contrast Definition

As it was pointed out in the last section, the Contrast Definition at a a% field defined in eq. 2.3 must be uniform among different kilovolt and tube current (dose) setups. Nevertheless, there is a –naturally– inconstancy in low contrasts signals due to several parameters, as scanner design, detector configuration, background radiation absorbed, FOV's, table configuration and kernels. In order to quantize this lack of constancy in the contrast definition at different dose stacks, it is followed here the next definition.

Let be $G_a(D_i)$ the corresponding contrast definition at the a% field for the dose D_i and $S_a = \{G_a(D_i) \setminus i = 1..M\}$ for some number of measures M. Then the *percent of instability*, is defined as:

$$U = 100\frac{StDev(S_a)}{Mean(S_a)} \tag{3.2}$$

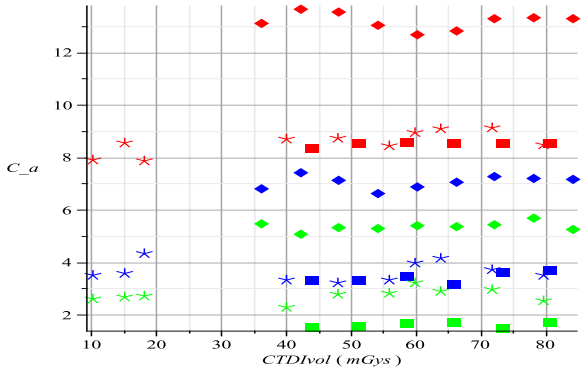

Figure 3-2: Contrast against CTDIvol (in mGys) from data sets processed by the Definition^{TM} (*asterisks*), Emotion 16^{TM} (*squares*) and Volume Zoom^{TM} (*diamonds*) systems in Head FOV. The kernel H30S was used for the reconstruction. As well as in Figure 3-1, the color key is red for the 1 % contrast fields, blue for 0.5 % and green for the 0.3 %.

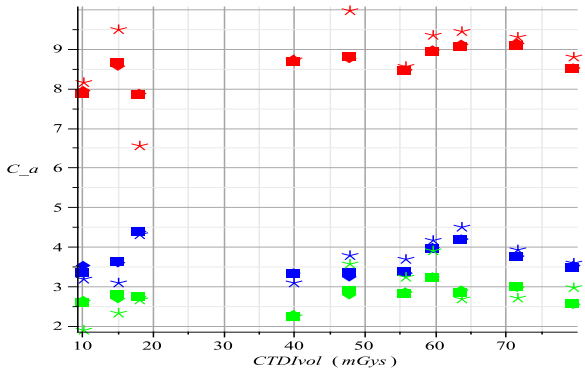

Figure 3-3: Contrast against CTDIvol (in mGys) from Definition^{TM} data sets reconstructed by H60S (*asterisks*), H31S (*squares*) and H30S (*diamonds*) in Head FOV. As well as in Figure 3-1, the color key is red for the 1 % contrast fields, blue for 0.5 % and green for the 0.3 %.

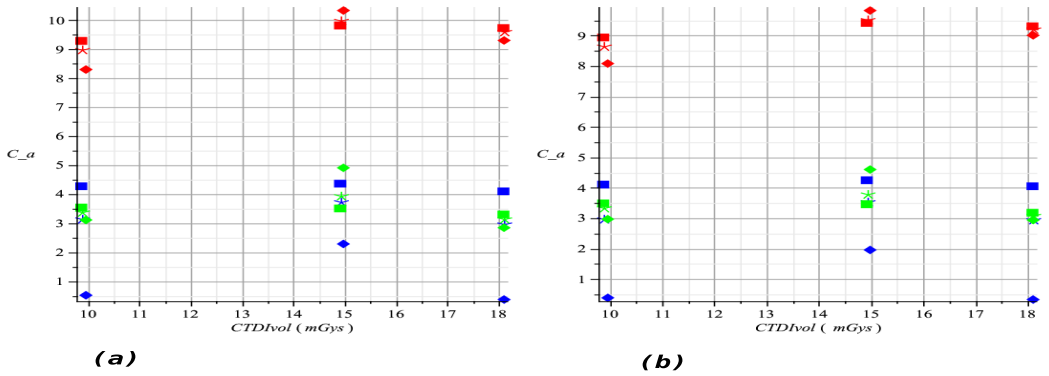

Figure 3-4: **(a)** Contrast against CTDIvol (in mGys) from Definition^{TM} data sets the generated by the source at 80 kV (*diamonds*), the one at 140 kV (*squares*) and *both* –the *Dual*– (*asterisks*) in Head FOV. B30F was used as kernel. **(b)** B31F is here the reconstruction kernel. Once again: red for the 1 % contrast fields, blue for 0.5 % and green for the 0.3 %.

where $StDev\,(S_a)$ is the standard deviation of the set S_a and $Mean\,(S_a)$ its mean value.

From Figure 3-5 to 3-6 the Instability Porcent is shown for the sets of measures of section 3.1.1. Figure 3-5 compares the inconstancy in the contrast definition values that are shown in Figure 3-1 of the Somaton^{TM} series in Abdomen FOV. In Figure 3-6, it is compared the different instability in the definition of contrast between the scanner in Head FOV, in Figure 3-7 between kernels in single-mode Definition^{TM} and in Figure 3-8 between 80 kV, 140 kV and *dual*-source-generated.

3.2.3 Noise Definition

As it is shown in [9], Noise Definition at the a% contrast field N_a goes as $\propto\ 1/\sqrt{I}$, where I is tube current and accordingly to the dose D. The significant quantity R_a (Signal-to-Noise Ratio) only is well-defined if the both the Contrast Definition is uniform among differernt dose values and the Noise Definition is follows a inverse-square-root law. Hence, a series of the noise computations were made in order to test the behavior of the noise residual signals all over the stacks. In general, the inverse-square-root law is qualitatively followed by the data sets, so the value of the Signal-to-Noise Ratio depends only in the sometimes ill-defined stability of the Contrast Definition. The Noise Definitions plots are shown in Figures 3-9 to 3-12.

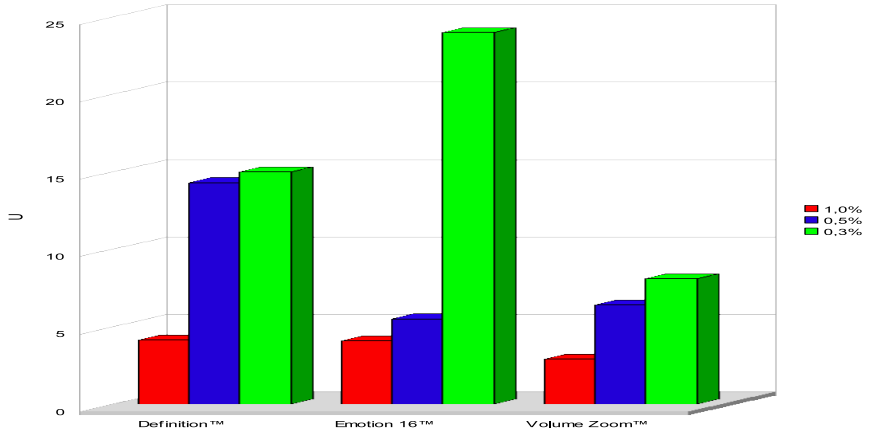

Figure 3-5: Comparing the Instability Porcent in the Contrast Field between stack sets generated by the scanners under examination, all reconstructed with the B30F kernel in Abdomen FOV.

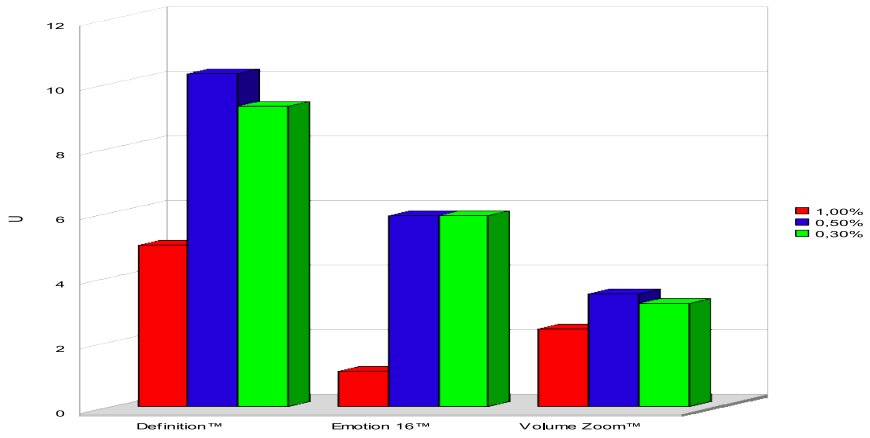

Figure 3-6: Instability Porcent in the Contrast Field between stack sets generated by the scanners under examination, all reconstructed with the H30S kernel in Head FOV.

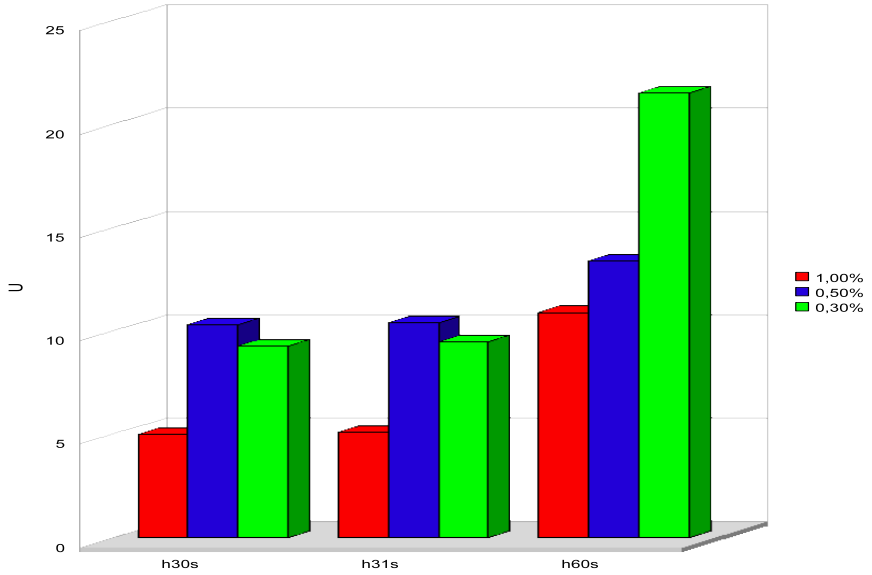

Figure 3-7: Instability Porcent in the Contrast Field between stack sets recontructed by several kernels in the Definition^{TM} system in Head FOV.

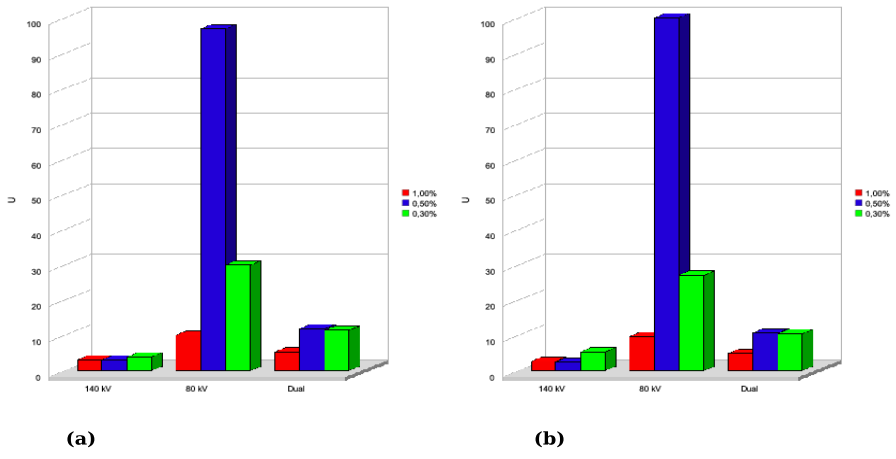

Figure 3-8: **(a)** Comparing the Instability Porcent in the Contrast Field between the stack sets generated by $80\,kV$, $140\,kV$ and *dual* sources and reconstructed by (a) B30F and textbf(b) B31F kernels in the Definition^{TM} system in Head FOV.

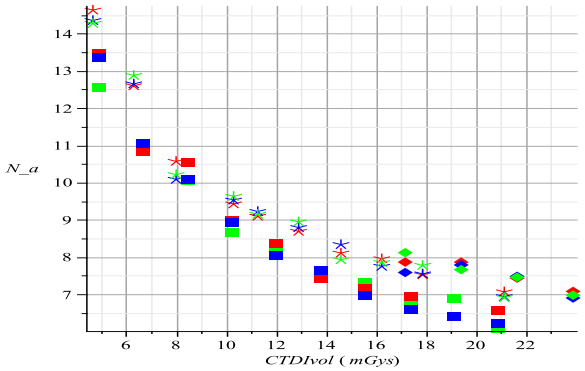

Figure 3-9: Noise against CTDIvol (in mGys) from data sets processed by the Definition^{TM} (*asterisks*), Emotion 16^{TM} (*squares*) and Volume Zoom^{TM} (*diamonds*) systems in Abdomen FOV. The kernel B30F was used for the reconstruction. The color key is red for the 1 % contrast fields, blue for 0.5 % and green for the 0.3 %.

3.2.4 Signal-to-Noise Ratio

Signal-to-noise ratio (or *STN*) is a measure of how much information available is distingishable from undesired signals. Nevertheless, although it is an usual parameter in standard quality assurance of diagnostics systems, it can be meaningfull only if there is a considerable constancy in the contrast and a well-behaved noise as it was mentioned in the previous section. Hence, the following plots which the SNR of Definition^{TM}in various setups (Figures 3-13 to 3-16 could not be considered as very reliable because of its rather unexpected instability, unlike some other works were the same approach to image quality analysis was employed ([10]). Therefore, any dose considerations based on the SNR measured in the present work must be taken with care. Nevertheless, some conclusions can be extracted from them. In the next chapter, a simple and qualitative reasoning called the *dose limit based on SNR rate*, based on the shape of the SNR curve, is proposed to argue possible optimal conditions of image quality and radiation protection.

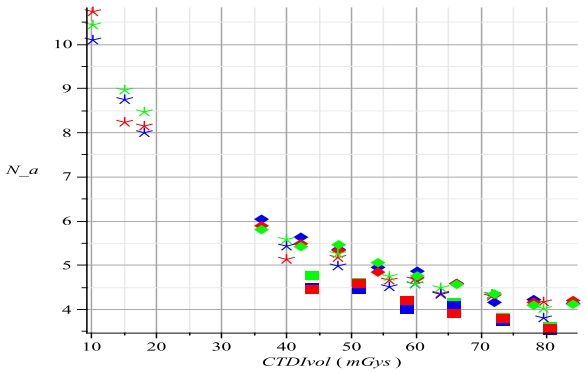

Figure 3-10: Noise against CTDIvol (in mGys) from data sets processed by the Definition^{TM} (*asterisks*), Emotion 16^{TM} (*squares*) and Volume Zoom^{TM} (*diamonds*) systems in Head FOV. The kernel H30S was used for the reconstruction. As well as in Figure 3-1, the color key is red for the 1 % contrast fields, blue for 0.5 % and green for the 0.3 %.

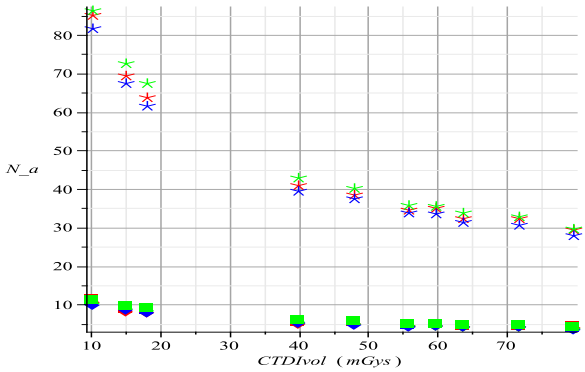

Figure 3-11: Noise against CTDIvol(in mGys) from Definition^{TM} data sets reconstructed by H60S (*asterisks*), H31S (*squares*) and H30S (*diamonds*) in Head FOV. As well as in Figure 3-1, the color key is red for the 1 % contrast fields, blue for 0.5 % and green for the 0.3 %.

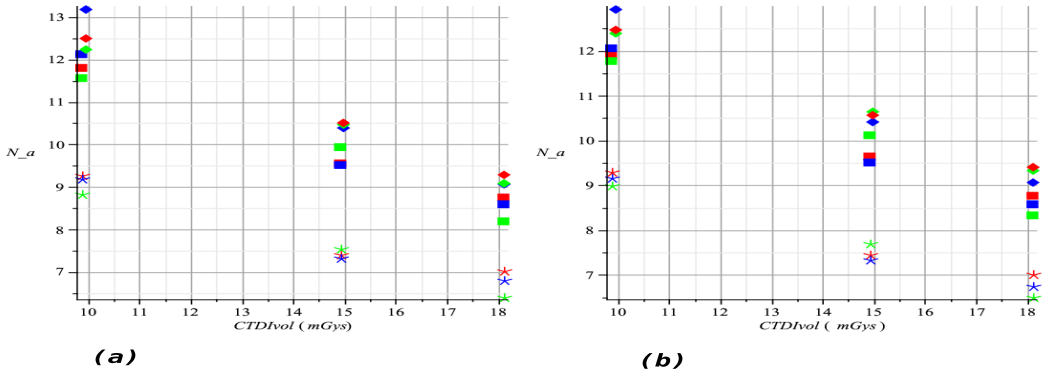

Figure 3-12: **(a)** Noise against CTDIvol(in mGys) from Definition^{TM} data sets the generated by the source at 80 kV (*diamonds*), the one at 140 kV (*squares*) and *both*–the *Dual*– (*asterisks*) in Head FOV. B30F was used as kernel. **(b)** B31F is here the reconstruction kernel. Once again: red for the 1 % contrast fields, blue for 0.5 % and green for the 0.3 %.

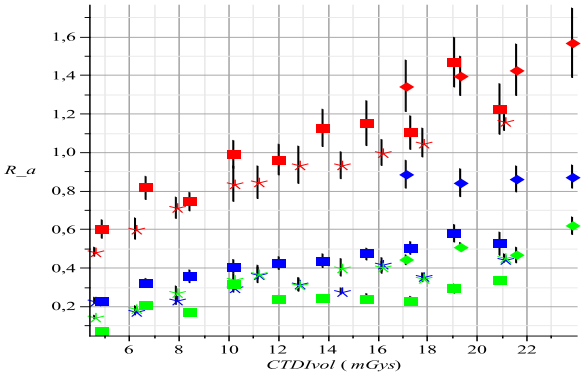

Figure 3-13: Signal-to-noise ratio against CTDIvol(in mGys) from data sets processed by the Definition^{TM} (*asterisks*), Emotion 16^{TM} (*squares*) and Volume Zoom^{TM} (*diamonds*) systems in Abdomen FOV. The kernel B30F was used for the reconstruction. As well as in Figure 3-1, the color key is red for the 1 % contrast fields, blue for 0.5 % and green for the 0.3 %.

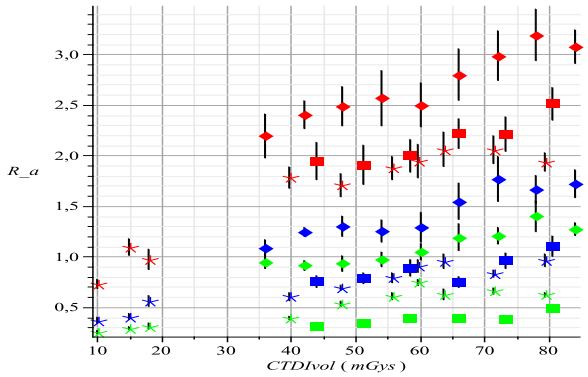

Figure 3-14: Signal-to-noise ratio against CTDIvol (in mGys) from data sets processed by the Definition^{TM} (*asterisks*), Emotion 16^{TM} (*squares*) and Volume Zoom^{TM} (*diamonds*) systems in Head FOV. The kernel H30S was used for the reconstruction. As well as in Figure 3-1, the color key is red for the 1 % contrast fields, blue for 0.5 % and green for the 0.3 %.

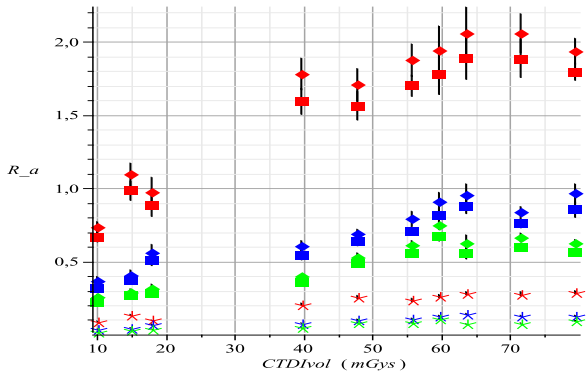

Figure 3-15: Signal-to-noise ratio against CTDIvol (in mGys) from Definition^{TM} data sets reconstructed by H60S (*asterisks*), H31S (*squares*) and H30S (*diamonds*) in Head FOV. As well as in Figure 3-1, the color key is red for the 1 % contrast fields, blue for 0.5 % and green for the 0.3 %.

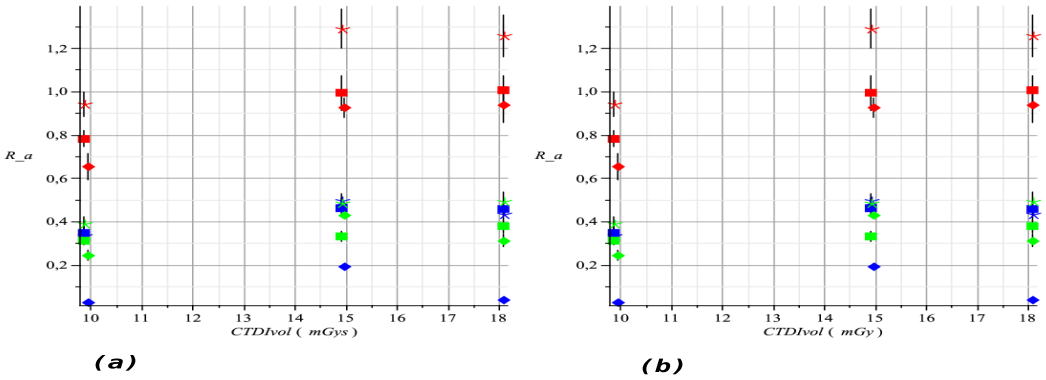

Figure 3-16: **(a)** Signal-to-noise ratio against CTDIvol (in mGys) from Definition^{TM} data sets the generated by the source at 80 *kV* (*diamonds*), the one at 140 *kV* (*squares*) and *both* -the *Dual set-* (*asterisks*) in Head FOV. B30F was used as kernel. **(b)** B31F is the reconstruction kernel here. Once again: red for the 1 % contrast fields, blue for 0.5 % and green for the 0.3 %.

3.3 High Contrast Tests

3.3.1 Profiles

High contrast tests in the present work, as explained in the Chapter 2, are twofold: to find the maximum resolution along the z-axis and on the xy-plane. The sample slide where the xy-plane analysis is performed is always that one with the highest maximum intensity inside a small ROI that contains the pulse signal bead. The system resolution is reported here by the Full Width at the Half Maximum ($FWHM$) of the point signal instead of the alternative method of the Modulation Transfer Function (see [9], p.102) or MTF, so the presentation of the result is rather straightfoward.

The measured bead signal FWHM's on the z-axis are shown in the Table 3.3 with the nominal values of resolution specified by Siemens® . In general there is a good improvement in the Definition^{TM}CT system if compared with the older Volume Zoom^{TM} and Emotion 16^{TM}. Further details of the z-axis profiles can be found in Figure 3-17. The expected contrast enhance in data sets reconstructed with "larger number" kernel is easily appreciated when it is compared Figure 3-17.a and 3-17.b.

In Table 3.4 it is shown the measured FWHM on the 2D bead signal. As it was described in detail in Chapter 2, the impulse signal was modeled as a gaussian two-dimensional function with

elliptical cross section (see Figure 3-18). The measured values presented in 3.4 are calculated with eq. 2.16 and the solution parameters of the model funtion in 2.9 . The FWHM's in this particular 2D problem are equal to the ellipse perimeter between the Pi, so they represent an "average spread" in every direction of the pulse signal. The resolution nominal values are computed by means of the "line pair per cm" values found in 2.1. In general, the resolution in the Definition^{TM} shows a backward step from its predecesors, an issue that will be further discussed in the next chapter.

Scanner, Kilovolt, Kernel	**FWHM**$_z$ (in mm) measured	**FWHM**$_z$ (in mm) nominal	
Definition^{TM} , 80 kV, B31F	0.76	0.60	
Definition^{TM} , 140 kV, B31F	0.75	0.60	
Definition^{TM} , *Dual*, B31F	0.76	0.60	
Definition^{TM} , 80 kV, B70F	0.71	0.60	
Definition^{TM} , 140 kV, B70F	0.98	0.60	
Definition^{TM} , *Dual*, B70F	0.76	0.60	
Emotion 16^{TM} , 130 kV, B70F	0.99	1.00	
Volume Zoom^{TM} , 120 kV, H45S	1.15	1.00	

Table 3.3: Measured and Nonimal Full Width at the Half Maximum in the z-axis for the three studied Somaton^{TM} CT systems.

Scanner, Kilovolt, Kernel	**FWHM**$_{xy}$ (in mm) measured	**FWHM**$_{xy}$ (in mm) nominal	
Definition^{TM} , 80 kV, B31F	1.32	0.48	
Definition^{TM} , 140 kV, B31F	1.26	0.48	
Definition^{TM} , *Dual*, B31F	1.22	0.48	
Definition^{TM} , 80 kV, B70F	1.23	0.48	
Definition^{TM} , 140 kV, B70F	1.23	0.48	
Definition^{TM} , *Dual*, B70F	1.23	0.48	
Emotion 16^{TM} , 130 kV, B70F	0.78	0.66	
Volume Zoom^{TM} , 120 kV, H45S	1.16	0.66	

Table 3.4: Measured and Nonimal Full Width at the Half Maximum in the xy-plane for the three studied Somaton^{TM} CT systems.

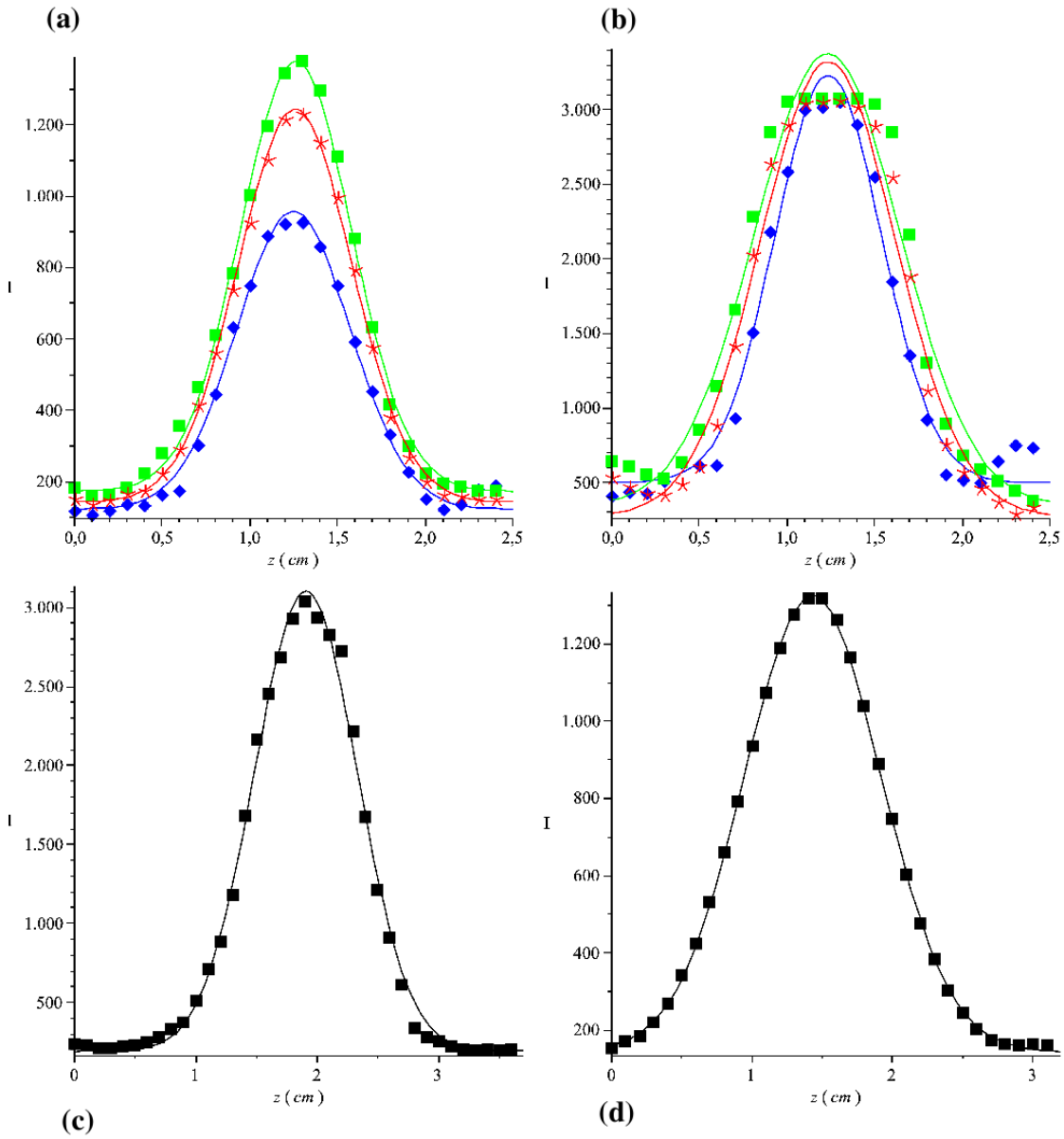

Figure 3-17: The z-axis profiles for Definition^{TM} **(a)** with image data reconstructed though B31F kernel, **(b)** with B70F, **(c)** Emotion 16^{TM} with B70F and **(d)** Volume Zoom^{TM} with H45S. Both profiles for the Definition^{TM} were measured with the system in dual source mode, so the color key is: red for *dual*, green for 140 kV and blue for 80 kV image sets. A important improvement in thin slice features is clearly seen in new generations Siemens® of CT systems.

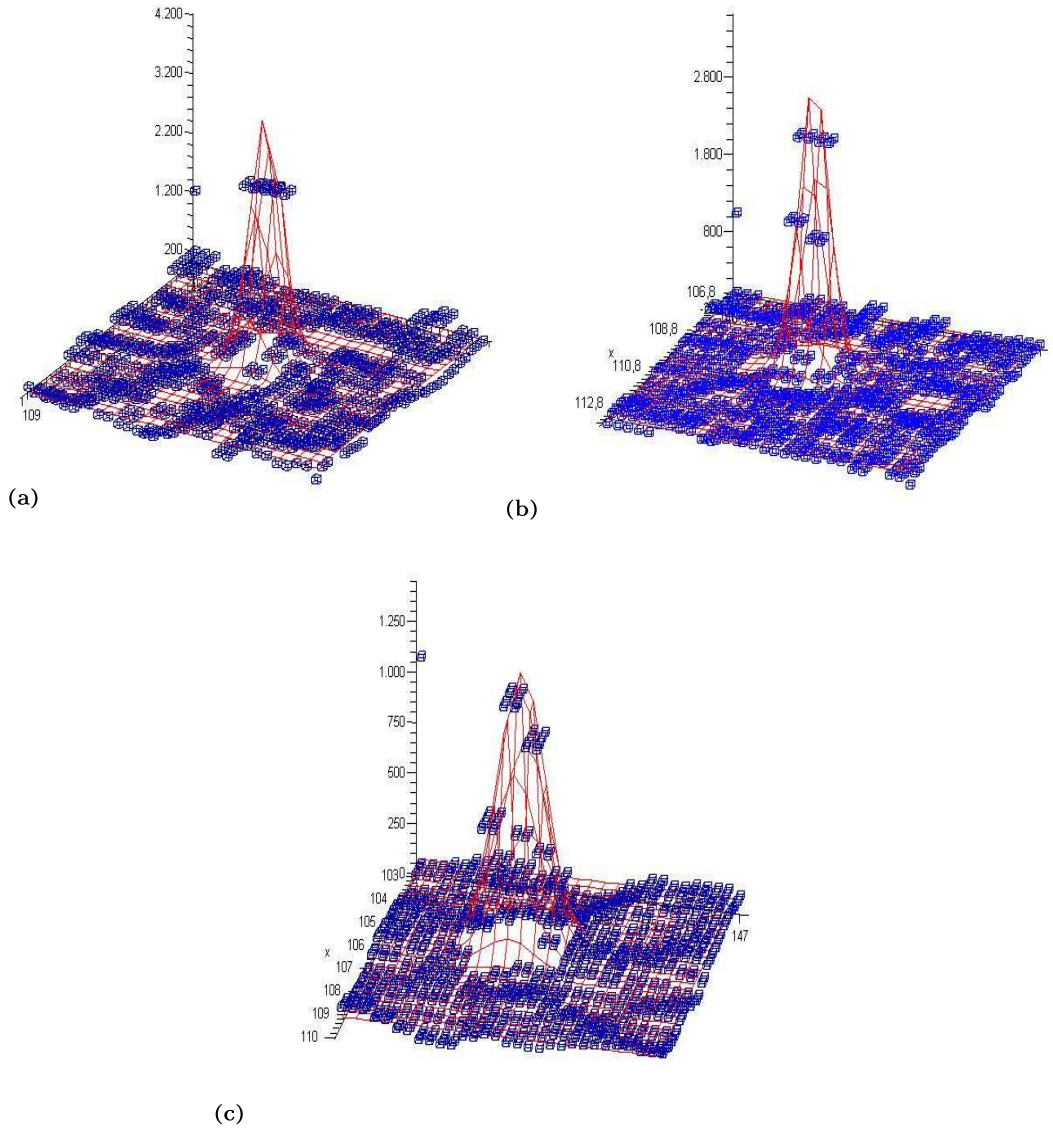

Figure 3-18: Here is shown the behavior of the intensity inside a small region that contains the bead pulse signal projection in the slide with the largest pixel value. The blue plots correspond to the actual intensity values obtained from the image and the red surfaces are the regressions generated by the model. The profile **(a)** comes from the dual B70F set produced by the Definition^{TM} **(b)** from the B70F Emotion 16^{TM} and **(c)** from B45S Volume Zoom^{TM}

3.3.2 Displacements between Image Sets in Dual Mode

The problem of displacements between the image sets obtained from the DSCT system is of primordial importance in CT Angiography and Cardiac CT because of the high precision demanded in small anatomical structures (in the millimeter scale) in those radiological procedures. In order to perform accurated diagnostic studies in DSCT clinical rutine, the displacement must be minimal, an difficult problem to solve both in the technical design of the scanner and in the implemented algorithms of computation.

This displacements are studied here by taking as a reference ROI the small bead signal. This impulse signal has some features like its tiny area, its high mean intensity value and its circle shape with a well defined radius (circular regions are invariant under rotations) that make it completely distinct from other CTP528 module structures. Inside the impulse region, its center is employed as a reference point because there is highest instensity value. In the Table 3.5 and , it is shown the location of the maximum intensity value for the Definition$^{\text{TM}}$ images sets as triplet (x_c, y_c, z_c) in tridimensional space. The coordinates in x and y direction are extracted from the xy-plane profile model function and the z coordinate is calculated in the z-profile fitting problem.

Kernel	80 kV	140 kV	*Dual*	
B31F	(105.09, 145.09, 1.25)	(105.16, 145.02, 1.26)	(105.14, 145.04, 1.25)	
B70F	(105.12, 145.09, 1.24)	(105.10, 145.05, 1.23)	(105.11, 145.06, 1.24)	

Table 3.5: Position of the highest intensity value in the 3D space (x_c, y_c, z_c) (in mm) for the 80 kV, 140 kV and *Dual* images sets obtained from Definition$^{\text{TM}}$ in dual source mode. The triplets of the maximum gray value presented here come from both reconstruction kernels used in this study. The x and y coordinates are extracted from the model funtion solution of the two dimensional bead signal distribution; the z coordinate is computed in the z-profile model function problem. These coordinates respresent the geometrical center of the bead as registered by the scanner. It is easy to see the exceptional matching for all the three set produced by each kernel, so it can be concluded that no signficant translation nor rotation takes place between the different data set from each tube.

Chapter 4

Discussion

4.1 Low Contrast Tests

4.1.1 Contrast Definition

Between Scanners in Single Mode

As it can be seen in Figures 3-1 and 3-2 the highest average contrast in the 1% field is produced by the Volume Zoom^{TM} (11.43 and 13.22 in abdomen and head FOV, respectively). The minor difference in the contrast in these two FOV modes is due to the soft tissue-oriented methodology the "H" type reconstruction algorithms is based. The contrast definition at the 1% field is, although, roughly 8.50 in both FOV for both the Emotion 16^{TM} and Definition^{TM} systems. It can be seen as a consequence of current state-of-the-art scanners with dozens of slices per rotation. In these systems, more background signal is produced by the scattering of X-rays between the detector arrays ([9]). So, on physical grounds, the smaller is the number of detectors, less scattered radiation occurs by the detector system. It can be argued that is why the 4-slice-per-rotation system Volume Zoom^{TM} can generate less noiser images than its more updated counterparts. So, although sytems like Volume Zoom^{TM} are slower than newer scanners, their image quality for soft tissue diagnostics is significantly superior.

When the nominal value of the field decreases, the behavior of the Definition^{TM} system is rather ambiguous: contrast of around 3 at the 0.5% and 0.3% ones is mostly indistinguishable (see Figures 3-1 and 3-2) at both abdomen and head views. This picture is more optimistic

for older generation scanners. For instance (Figure 3-1), with the Emotion 16^{TM} in abdomen setups, regions which electron densities that differ in a 0.5% will have differences in intensity of almost 4, and for Volume Zoom^{TM} the difference will be around 7. Due to the mathematical strategies specially designed for soft tissue in head kernels, these differences in gray values are larger in the older scanners (Figure 3-2), but the superposition of the contrast at the 0.5% and 0.3% fields still holds for the Definition^{TM} system. So, the number of detectors carries some impediments to generate images from objects with regions with little electron density differences.

Between Kernels in Single Mode Definition^{TM}

As it can be deduced from the kernel nomenclature in diagnostics CT systems, images reconstructed with the H60S kernel are naturally more sharper than those with H30S and H31S. So, it is easy to see why the images recontructed with H60S have a contrast definition at regions with 1% of electron density of 8.9, a slightly higher value than that of 8.6 reached by both the H30S AND H31S kernels (Figure 3-3). Although the contrast between regions of 1% density difference is still acceptable, the indistinguishability problem for regions with density differences lower than 1% holds almost invariant along the employed recontruction kernels.

In Dual Mode

The contrast values in dual mode are very similar to those from the Definition^{TM} in single source mode. For the 1% fields, contrast definition values are almost the same for the three types image stacks 3-4, but a clear energy-based differentiation can be seen in the 0.5%. High-penetrating X-rays from the 140 kV source has the top average contrast and low energetic radiation from the 80 kV tube has the smallest, as it is expected. In general, from nominal low contrast percent difference lower than 1%, the dual set contrast is somewhere in the middle between the values of the other source.

Nevertheless, there is interesting "anomaly" only present in the three stacks produced in dual mode. An anisotropy in the illumination makes possible a brighter posterior section of the phantom, therefore all the upper (anterior) part of the field of view has a slightly lower gray value. This feature can be seen even with simple eye review of the slide, as it is shown in Figure

4-1. This non-uniform illumination explains the unusual behavior of the contrast definition shown in Figure 3-4, where the contrast definition values in the 0.3% are higher than in the 0.5%. This apparent contradiction holds for both image stacks reconstructed by the B30F and B31F kernels. The issue of illumination in dual mode Definition^{TM} could be due (without any attempt of certainty) to scattered radiation from the patient (in this case, phantom) produced by the asymetric design of the tube positioning as it is shown in Figure 2-1. Although this anisotropy is very small, objects which electron density is less than 1% could not be adequately differentiated.

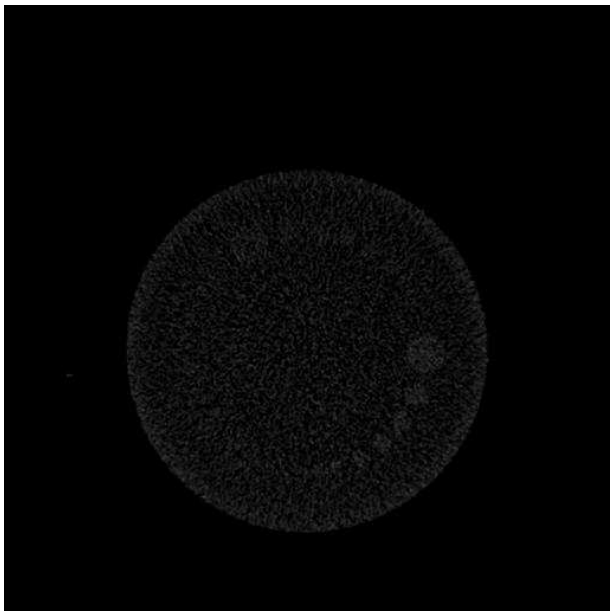

Figure 4-1: Sample slide of the CTP515 module produced by the Definition^{TM} in dual mode (tube kilovolt: 140 kV, CT dose density: 18.07 $mGys$, kernel B31F) where it can be appreciated an uniform illumation between the posterior and anterior part of the phantom. The anterior region (where the 0.3% fields are located) has slightly higher gray value than the posterior region, hence the 0.5% fields have a lower contrast definition than its 0.3% counterparts. This phenomena is only observed in dual mode.

4.1.2 Instability of the Constrast Definition

The contrast measures previously discussed showed how much is the intensity difference between the targets and its surrounding subtrate and how is its behavior between different scanner,

kernels and mode operations. The instabilility in contrast definition show how constant is the contrast along several dose densities. The constancy of the contrast definition would depend mainly in the design of the scanner. A more stable set of contrast measures is due to a internal design that minimize the re-scattering processes, as well as a adequate power management system that avoids current or voltage uncontrolled peaks.

In the abdomen FOV, the instability percent grows with nominal contrast value as it can be expected (Figure 3-5). Because of the increasing number of detector arrays in modern CT systems, the Definition^{TM} scanner produces the most instable contrast measures between $CTDIvol$ at every nominal contrast percent, although there is proof of a not enhanced very low contrast definition (v.b. at 0.3%) for the Emotion^{TM} 16 system. Hence, the most reliable CT scanner for abdomen studies in term of low contrast sensibility is the Volume Zoom^{TM}, with less than 9% of dispersion in the 0.3% fields.

In the head FOV (Figure 3-6) the picture for the Definition^{TM} does not change significantly. Its instability is raised in general but not in substantial way. This situation is also share with the Volume Zoom^{TM}. In the other half, Emotion 16^{TM} shows an extensive improvement from its predecessor with a outstanding stability in head studies.

In Figure 3-7, the instability in the contrast definition is compared between different head kernels with Definition^{TM} system in single mode. Since the H30S and H31S generate images with similar sharpness, it is natural that they share similar dispersions. The higher dispersion in the H60S set is due to its enhancement of the high intensity regions, which produces a distinct strenghten of the noise as a consequence.

Since the instability percent is indeed a statistical variable (eq. 3.2), its value as decisive and reliable physical measure depends on how much samples were taken. Because of this fact of the basic Statitical theory, it is natural that the percents shown in Figure 3-8 have some unusual values. Nevertheless, some important information can be extracted. As it can be expected, the lower dispersion is generally found in the 140 kV set, followed by the dual and then by 80 kV one. For the 1% targets, the stability is strongly improved in the 140 kV set when compared to those in single mode (from 5% to 3%). The stability in the dual set is regularly similar to those found in the single mode though. Nevertheless, there is an over-valued percent in both B30F and B31F images of the 80 kV set at the 0.5% target. It can be argued that it is due to the

recently commented illumination anisotropy of the dual-mode sets from the Definition^{TM} –an effect that is more strong in the 80 kV sets–, that makes that the ROI's at the 0.5% are almost the same (in terms of mean intensity and standard deviation) that the background ones, which are dominated mainly by noise. Therefore, the measure of the instability at these 0.5% targets is as random as that of the background.

4.1.3 Noise Definition and Signal-to-Noise Ratio

In general the noise is well behaved in all the analyzed series of stacks, it response to the dose in completely regular (from Figure 3-9 to 3-12). Noise in Emotion 16^{TM} and Volume Zoom^{TM} is almost completely overlapped, although it grew a little higher in sigle mode Definition^{TM} for both abdomen and head modalities (Figures 3-9 and 3-10). In Figure 3-11, the noise enhancement due to the recently discussed strong sharpening qualities of the H60S kernel is shown in very explicity way. In the case of the Definition^{TM} in dual mode, the dual sets show an outstanding noise reduction, even better than that of the 140 kV sets (Figure 3-12).

The contrast definition instability was defining factor that prevented the present work from pursuing a signal-to-noise based analysis. In general (Figures 3-13 to 3-16) signal-to-noise is not as regular as in other studies [10], so the descriptions and conclussions that are being exposed here are more qualitative and therefore not terminating.

Since the noise definition goes as $1/\sqrt{D}$ and the contrast is –theoretically– constant at the targets of the CT515 module, v.b. with no significant dependence on the dose (tube current), then the signal-to-noise ratio is proportional to $\sqrt{D}$. Because the change rate of the signal-to-noise ratio with respect to dose density (the derivative) goes as $1/\sqrt{D}$, it is possible to find a effective dose limit D_L where the signal-to-noise ratio will not increase at rate higher than $\eta = dR_a/dI|_{D_L} \propto 1/\sqrt{D_L}$. For dosis higher than D_L, the image quality (quantized by the signal-to-noise ratio) will not be significantly increased. By this method of the dose limit, standard CT sytems setups which comprise mininal dose with optimal image quality can be proposed.

The issue of scattering in complex detector arrays is clearly shown in Figures 3-13 and 3-10, where the old fashioned 4-slices-per-rotation Volume Zoom^{TM} leads both the abdomen and head studies in the SNR's at the 1% contrast targets. Based on the shape of the curve drawn

by the plots, a cut-off dose $CTDIvol_L$ can be set in the range between 19 and 22 $mGys$ for abdomen studies (because only in this range the SNR reaches a value greater than 1.0) and 40 and 50 $mGys$ in head FOV for the Definition^{TM} system in single mode. The fact that no SNR in the 0.5% and 0.3% contrast targets reachs the value of 1.0 –so noise is a dominant factor within them– means that the lowest density difference that any Somaton^{TM} series scanner can process is precisely 1.0%. Nevertheless, for the specific case of the newly realeased Definition^{TM}, its lowest (electron) density is even greater than that, probably between 1.5% and 2.0%.

In Figure 3-15 it is shown the behavior of SNR between several kernels in Definition^{TM} single mode. The features of the H60S reconstruction proves a widely noise dominated images –where the top is less 0.3– and the overall values of the H30S are slightly larger than those of the H31S as it was expected.

The SNR's in the dual mode stacks are not very different from those ones in single mode Definition^{TM} (Figure 3-16). In general, the dual sets obtained the best results. Although more sample data is necessary to propose a stronger argument, the cut-off dose D_L for dual mode can set in the range of 14 to $CFDI_{vol}$, because there is where the dual sets reach the optimal SNR in terms of image quality and radiation protection. For both B30F and B31F reconstructions, no 80 kV or 140 kV set surpassed 1, so the noise in general competes in equal terms with effective X ray signals.

4.2 High Contrast Tests

Because of the detector multi-array-oriented designing in modern Siemens® CT systems, features like thiner slices and faster full bodies scans are improved in every new model with that trademark. In terms of z-axis resolution, the Definition^{TM} system has subtantially overcame its older counterparts. As can be seen in the Table 3.4, the resolution with body kernels in Definition^{TM} has almost doubled the one its close "relative" Volume Zoom^{TM}. The Definition^{TM} z-axis resolution is even better than the one of the Emotion 16^{TM} approximately by 25 mm. Due to its sharpening characteristics and noise amplification, the B70S kernel affects the spread of the pulse function and therefore, the resolution is higher than in its analogous B31S series of stacks.

In contrast to its z-axis resolution, the Definition$^{\text{TM}}$ xy-plane resolution has stepped backwards (Table 3.4). With a average of 1.24 mm for all the dual mode series of stacks (with both studied kernels), the Definition$^{\text{TM}}$ is still no match in terms high-detailed efficience to the Emotion 16$^{\text{TM}}$. The very feature that ensures a highly developed resolution in the z-axis –the multi-detector system which produces 64 slices per rotation– seems to be the main reason of the decrease in the resolution in the xy-plane. As it was several times noted in the previous low contrast tests section, Definition$^{\text{TM}}$ images are more noisy than the ones of the other Somaton$^{\text{TM}}$ series models. Therefore, the noisy behavior due to a relative large re-scattering in the detectors widens the bead impulse signal to widen more.

About the matching problem between the three dual mode sets from the Definition$^{\text{TM}}$, the maximal separation of bead center between two stacks (for instance, the 140 kV and the *dual* ones) is in the order of 0.1 mm (see Table 3.5). If the minimal xy-plane resolution that can be achieve by the Definition$^{\text{TM}}$ is roughly 1.2 mm, then the offset between similar points in different stacks will 10 times less than the resolution of the scanner itself. Consequently and without any reasonable doubts, it can be affirmed that the matching of the three differents stack generated by the Definition$^{\text{TM}}$ system match in a practically perfect way.

Chapter 5

Conclusions

The Definition^{TM} is novell CT systems with several new features that make it an attractive choice for the radiology specialist in the present times. Although, it also has some backwards characteristics that make it inadequate to certain clinical studies. The final purpuse of this study is to uncover these pros and cons. At the end of the present study, it can be set as summary that:

- The contrast definition in the Definition^{TM} DSCT system (both in single and dual source mode) is comparable with that of the Emotion 16^{TM} but lower that the one of the Volume Zoom^{TM}.
- Due to re-scattering in the large detector system, the Definition^{TM} suffers the largest instability in the contrast definition between the tested scanners. The Emotion 16^{TM} shows a quite good constancy in that image parameter.
- There is a observed non-uniform illumation present in all the dual source mode stacks which altered the pixel values of the background. The presence of this anisotropy is more dominant the faint stack generated by the less energetic source.
- Definition^{TM} Noise presence is larger than in its previous counterparts, a fact that makes difficult to distinct regions with electron density differences of 1% or less with doses usually employed in radiology rutine with other CT systems.

- In the dual source mode, the *Dual* stack is generally the one where more low contrast differentiation can be done.
- Because of the large array detector system and its precise mechanical design, the Definition^{TM} z-axis resolution has been succesfully improved beyond the limits of the older Somaton^{TM} models.
- The xy-plane resolution of the Definition^{TM} is affected by the large noise influence due the re-scattering. In terms of xy-plane resolution, the best option still is the Emotion 16^{TM}.
- The matching between the three stacks generated in the dual mode problem can be completely negligible.

The Definition^{TM} system is very fast CT system that is extremely useful in Cardiac CT –because of its high temporal resolution which falls within the range of the cardiac cycle– and in CT Angiography –because of its high speed that enables the physician to obtain real time snapshots–. Nevertheless, in order to obtain the largest amount of advantages with the minimal costs, its employ must have certain mild restrictions. Due its noise dominated features, its use in detailed soft tissue differentiation –like in tumor studies– and small object determination (with sizes under $1.5mm$) must be prevented.

Dual source computer tomography is a relatively new application in medical practice. In order to exploit its capabilities, more research must be done. The consequences of re-scattering in large detector arrays must be adequately modeled and quantized, as well as its repercutions in structures with small electron density differences. The issue of the anisotropy must studied in much more detail. Although the problem of matching is not an important issue at this time, it will be a very important factor in next generation scanner with resolutions down the *half-milimeter* scale.

Bibliography

[1] T.G. Flohr et al. *First Perfomance evaluation of a dual-source CT. (CSCT) system.* **Eur Radiol** (2006) **16**:256.

[2] S. Achenbach et al. *Contrast-enhanced coronary artery visualization by dual-source computed tomography—Initial experience.* **Eur J Radiology** (2006) **57**:331

[3] D. Matt, H. Scheffel, S. Leschka, T.G. Flohr, B. Marincek, P.A. Kaufmann3 and H. Alkadhi. *Dual-Source CT Coronary Angiography: Image Quality, Mean Heart Rate, and Heart Rate Variability.* **Am J Roetgenology** (2007) **189**:567.

[4] S. Achenbach, K. Anders, W. Kalender. *Dual-source cardiac computed tomography: image quality and dose considerations.* **Eur Radiol** DOI 10.1007/s00330-008-0883-3.

[5] T. Flohr, K. Stierstorfer, S. Ulzheimer, H. Bruder, A. Prinak, C McCollough. *Image reconstruction and image quality evaluation for a 64-slice CT scanner with z-flying focal spot.* **Med Phys** (2004) **32**:2536.

[6] T. Flohr, K. Stierstorfer, R Raupach, S. Ulzheimer, H. Bruder. *Performance evaluation of a 64-slice CT-system with z-flying focal spot.* **Röfo Fortsch Geb Rontgenstr Neuen Bildgeb Verfahr** (2004) **176**:1803.

[7] P. Schardt, J Deuringer, J. Freundenberger, E. Hell, W. Knuepfer, D. Mattern, M. Schild. *New X-ray tube performance in computed tomography by introducing the rotating envelope tube technology.* Med Phys (2004) **31**:2699.

[8] D. J. Goodenough. *Catphan® Manual.* The Phantom Laboratory. New York. 2005.

[9] W. A. Kalender. *Computed Tomography*. 2nd ed. Publicis. Erlagen. 2005.

[10] G. Weisser, K.J Lehmann, R Scheck, E. Coppenrath, M. Georgi. *Dose and image quality of electron-beam CT compared with spiral CT*. **Invest Radiol** (1999) **34**:415.

[11] W.S Rasband. *ImageJ*. U. S. National Institutes of Health, Bethesda, Maryland, USA, http://rsb.info.nih.gov/ij/, 1997-2008.

[12] M.D. Abramoff, P.J. Magelhaes, S.J. Ram. *Image Processing with ImageJ*. **Biophotonics Int** (2004) **11**:36.